Supporting Information

Sulfur-Driven Transition from Vertical to Lateral Growth of 2D SnS-SnS_2 Heterostructures and Their Band Alignments

Yecheng Cheng,[†] Pengtao Tang,[†] Pei Liang,[†] Xueyin Liu,[‡] Dan Cao,[‡] Xiaoshuang Chen,[§] and Haibo Shu[†,*]

[†]College of Optical and Electronic Technology, China Jiliang University, 310018 Hangzhou, China

[‡]College of Science, China Jiliang University, 310018 Hangzhou, China

[§]National Laboratory for Infrared Physics, Shanghai Institute of Technical Physics, Chinese Academy of Science, 200083 Shanghai, China

[*]Corresponding author. Phone: +86-0571-86875622, E-mail: shuhaibo@cjlu.edu.cn

S1. Experimental setup and parameters of CVD growth.

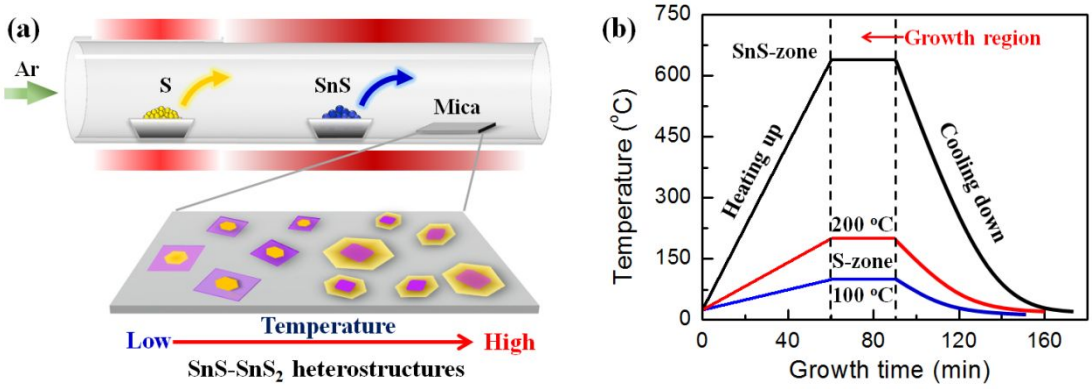

Figure S1. (a) Schematic diagram for the CVD setup for the growth of SnS-SnS_2 heterostructures. The inset is a schematic view of mica substrate with growing 2D SnS-SnS_2 heterostructures under different growth temperatures. (b) Temperature evolution of the reaction furnace. The black curve indicates the temperature evolution of SnS (or high-temperature) heating zone, and blue and red curves correspond to the lower and upper limit of S-zone temperature (T_S), respectively.

Table S1. **The Experimental Parameters and the Corresponding Products**

Here the products of SnS, SnS_2/SnS, SnS/SnS_2, and SnS_2 denote that growing 2D structures are SnS nanosheets, SnS_2/SnS vdW heterostructures, SnS/SnS_2 core-shell heterostructures, and SnS_2 flakes, respectively.

Samples No.	SnS	S	T_{SnS}	T_S	Carrier gas (Ar)	Growth time	Products
1	150 mg	150 mg	640 ˚C	110 ˚C	300/60 sccm	30 min	SnS (100%)
2				140 ˚C			SnS (18%) SnS_2/SnS (82%)
3				180 ˚C			SnS/SnS_2 (88%) SnS_2 (12%)
4				200 ˚C			SnS_2 (100%)
5	150 mg	50 mg	640 ˚C	140 ˚C	300/60 sccm	30 min	SnS (44%) SnS_2/SnS (56%)
6		150 mg					SnS (18%) SnS_2/SnS (82%)
7		250 mg					SnS (11%) SnS_2/SnS (80%) SnS/SnS_2 (6%) SnS_2(3%)
8		350 mg					SnS (3%) SnS_2/SnS (76%) SnS/SnS_2 (13%) SnS_2(8%)
9	150 mg	50 mg	640 ˚C	180 ˚C	300/60 sccm	30 min	SnS_2(8%) SnS/SnS_2 (92%)
10		150 mg					SnS_2(12%) SnS/SnS_2 (88%)
11		250 mg					SnS_2(26%) SnS/SnS_2 (74%)
12		350 mg					SnS_2(46%) SnS/SnS_2 (54%)

S2. The SOC effect on band structures of SnS_x nanosheets

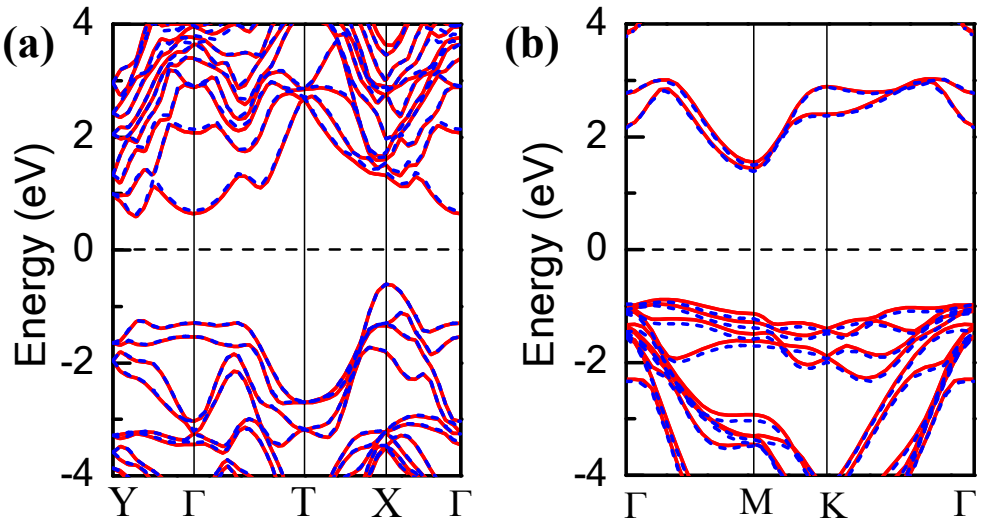

Figure S2. Band structures of bilayer (a) SnS and (b) SnS_2 nanosheets calculated using the HSE06 functional with (in red) and without (in blue) the SOC. The position of Fermi level is set to the zero-point of energy.

S3. AFM images of growing 2D structures with different T_S

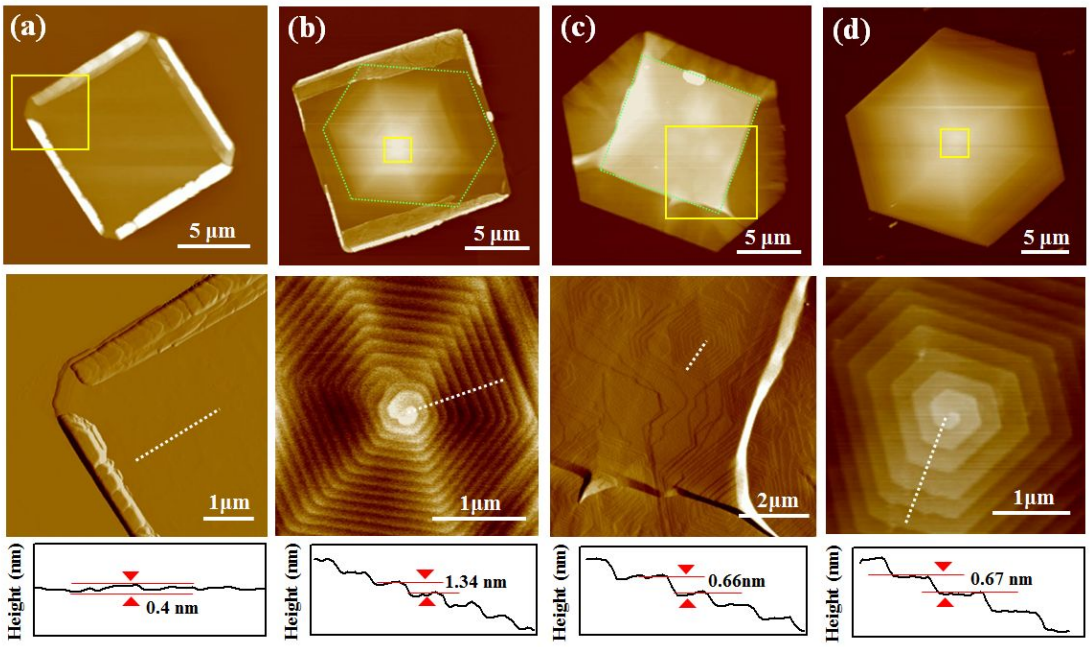

Figure S3. AFM images of 2D (a) SnS, (b) vertical SnS_2/SnS vdW heterostructure, (c) SnS/SnS_2 core-shell heterostructure, (d) SnS_2 flake. Upper panels, middle panels,

and lower panels indicate the complete AFM images, enlarged AFM images in the yellow frame regions, and height profiles along the white dash lines of these 2D flakes. The green frames in b and c show the central SnS_2 and SnS grain in the heterostructures, respectively.

S4. The statistics of growing 2D structures with different T_S

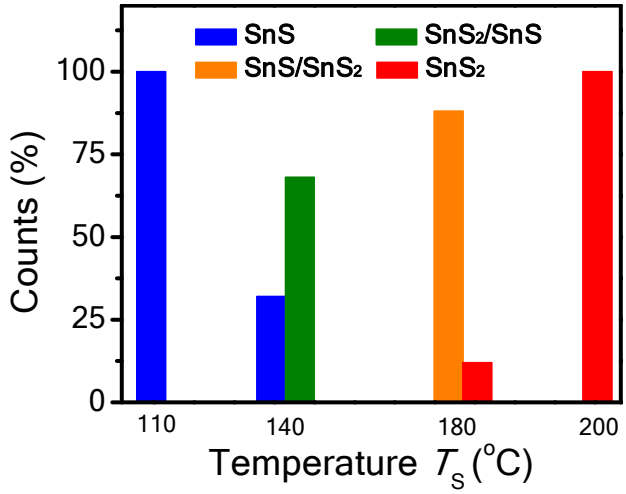

Figure S4. The statistics of growing 2D structures with different S-zone temperatures (T_S). SnS, SnS_2/SnS, SnS/SnS_2, and SnS_2 represent that growing 2D structures are SnS nanosheets, SnS_2/SnS vdW heterostructures, SnS/SnS_2 core-shell heterostructures, and spiral SnS_2 flakes, respectively.

S5. Role of S-powder amount in the growth of SnS-SnS_2 heterostructures

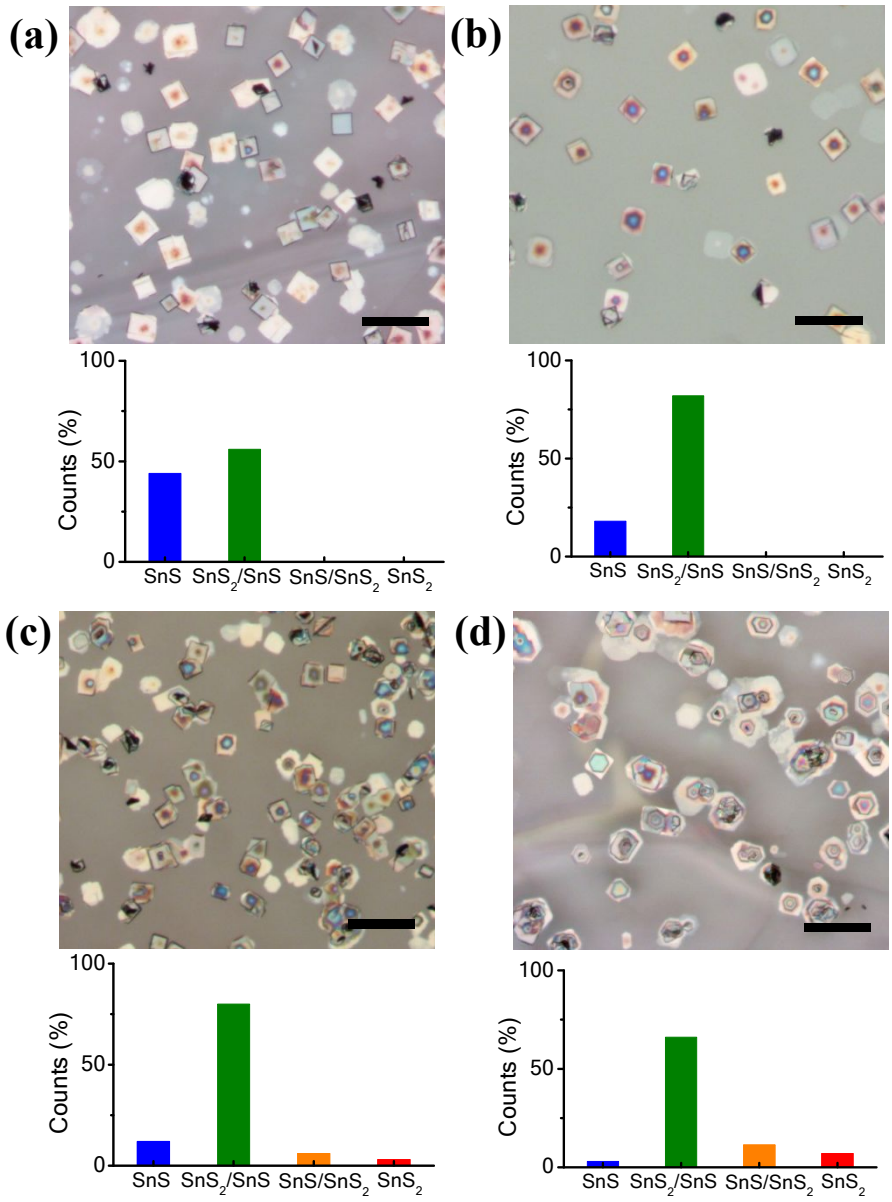

Figure S5. The OM images and statistics of the proportion of various formed 2D structures grown with (a) M_S = 50 mg, (b) M_S = 150 mg, (c) M_S = 250 mg, (b) M_S = 350 mg at T_S = 140 ˚C. The scale bar is 60 μm. Here SnS, SnS_2/SnS, SnS/SnS_2, and SnS_2 represent that growing 2D structures are SnS nanosheets, vertical SnS_2/SnS heterostructures, SnS/SnS_2 core-shell heterostructures, and spiral SnS_2 nanoplates, respectively.

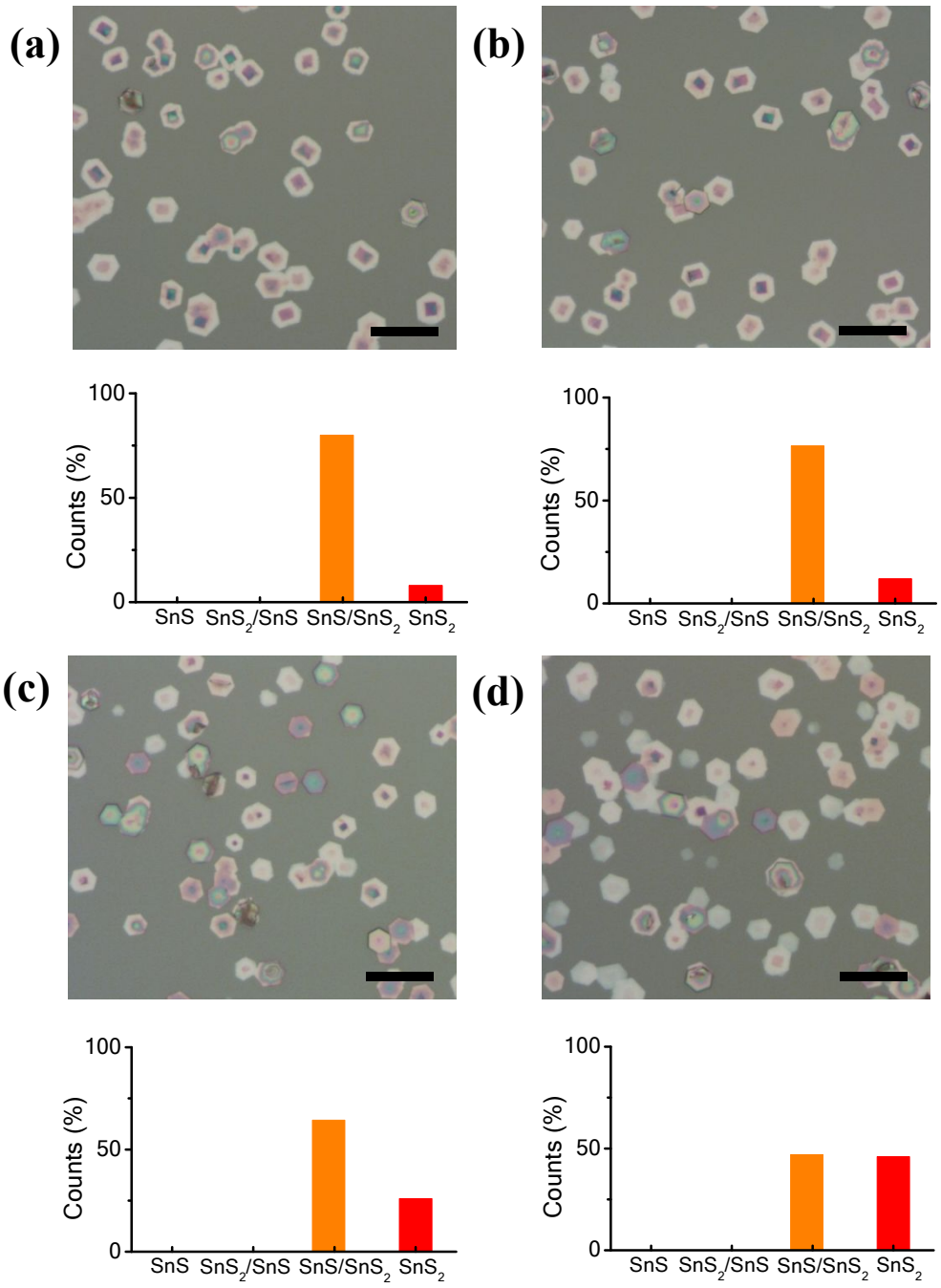

Figure S6. The OM images and statistics of the proportion of various formed 2D structures grown with (a) M_S = 50 mg, (b) M_S = 150 mg, (c) M_S = 250 mg, (b) M_S = 350 mg at T_S = 180 ˚C. The scale bar is 60 μm. Here SnS, SnS_2/SnS, SnS/SnS_2, and SnS_2 represent that growing 2D structures are SnS nanosheets, vertical SnS_2/SnS heterostructures, SnS/SnS_2 core-shell heterostructures, and spiral SnS_2 nanoplates, respectively.

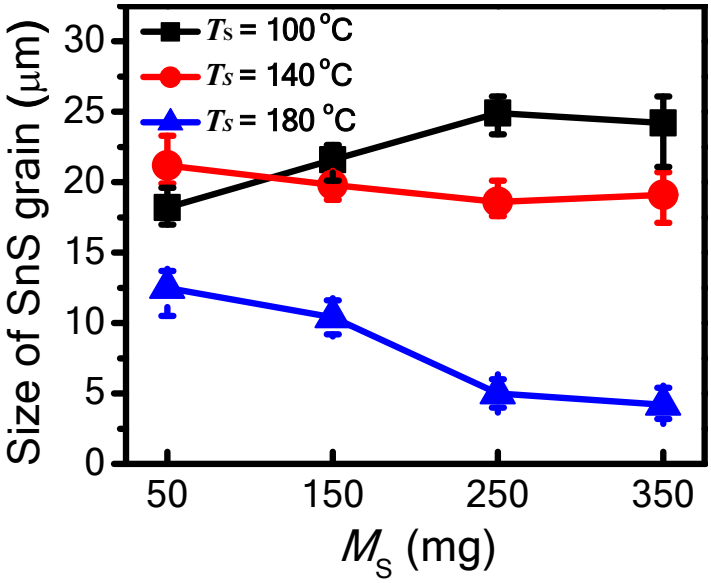

Figure S7. The size of SnS grains in the formed 2D structures as a function of sulfur-powder amount (M_S) at the sulfur-zone temperature (T_S) of 100, 140, and 180 ˚C.

S6. Atomic structures and shape evolution of SnS and SnS_2 edges

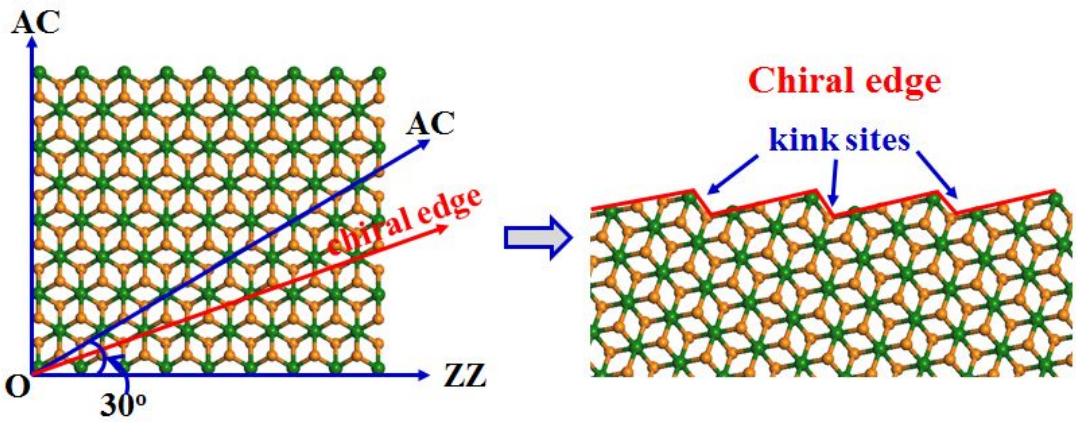

Figure S8. The atomic structure of chiral SnS_2 edges. The chiral edge includes a large number of kink sites that are active for the rapid growth of SnS_2.

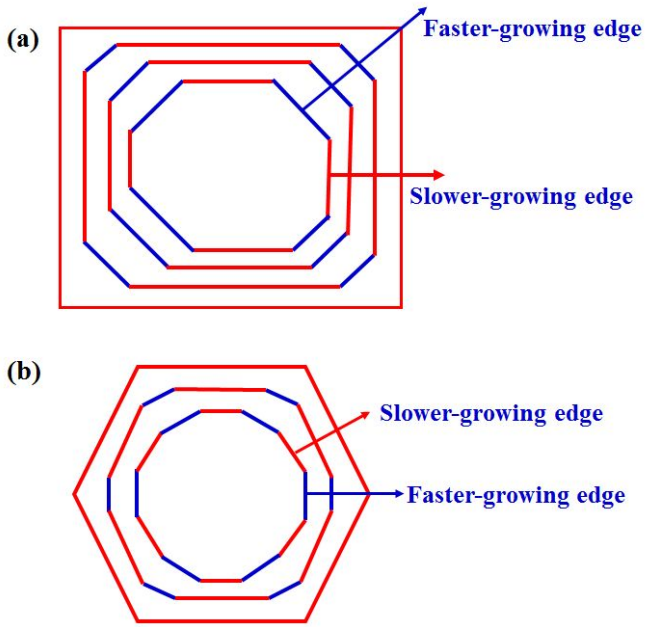

Figure S9. Morphological evolution of (a) SnS and (b) SnS_2 domains based on the kinetic Wulff construction. In the growth process, the edges with fast growth rate disappear and the domain morphology is thus determined by the slow-growing edges.

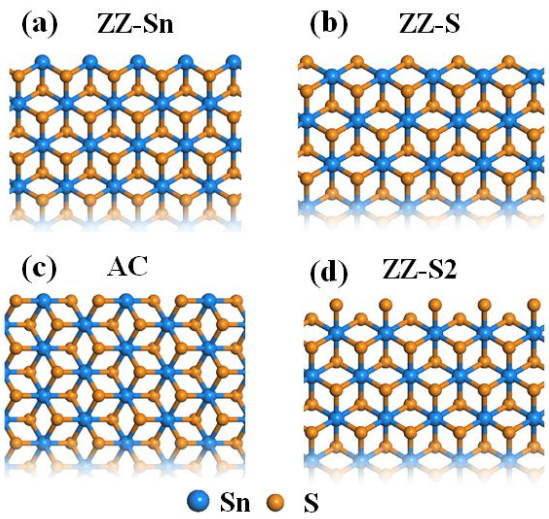

Figure S10. Atomic structures of four typical SnS_2 edges: (a) Sn-terminated zigzag edge (ZZ-Sn), (b) S-terminated zigzag edge (ZZ-S), (c) armchair edge (AC), and (d) S_2-terminated zigzag edge (ZZ-S_2). The blue and orange balls represent Sn and S atoms, respectively.

S7. HRTEM characterization of vertical SnS_2/SnS heterostructure

In order to reveal the morphology and interfacial structure of vertical SnS_2/SnS heterostructures, TEM characterization was carried out. As shown in Figure S11a, it can be seen that the synthesized SnS_2/SnS heterostructure is composed of a large SnS grain located at the bottom layer and a smaller and thicker SnS_2 grain on the top of the SnS grain. The high-resolution TEM (HRTEM) micrograph shown in Figure S11b displays that the interplane distance of 0.29 and 0.32 nm, which corresponds to the (101) plane of SnS and (100) plane of SnS_2, respectively. Moreover, there is a distinct boundary between SnS and SnS_2, indicating that the SnS_2/SnS interface is sharp.

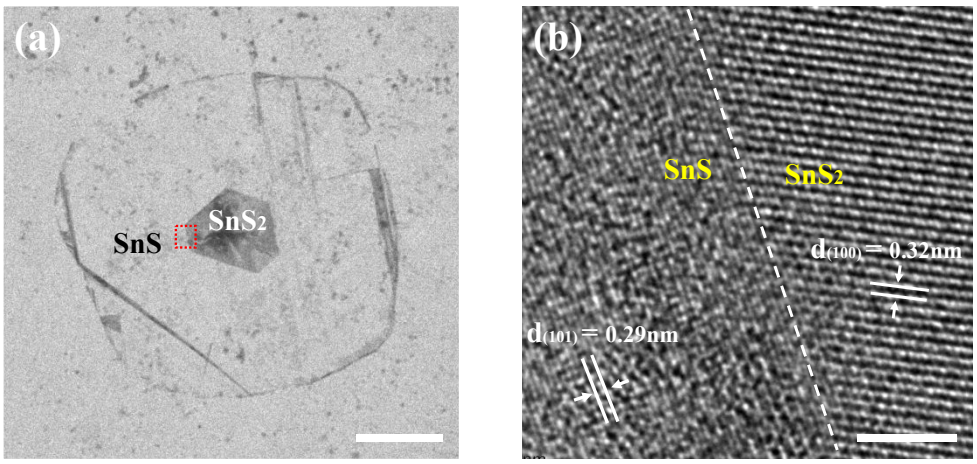

Figure S11 (a) Low-resolution TEM image of vertical SnS_2/SnS heterostructure. The scale bar is 4 μm. (b) HRTEM image of SnS/SnS_2 interface in the heterostructure taken on the region marked by the red dash frame in (a). The scale bar is 2 nm.

S8. Interfacial stress of SnS/SnS_2 core-shell heterostructures.

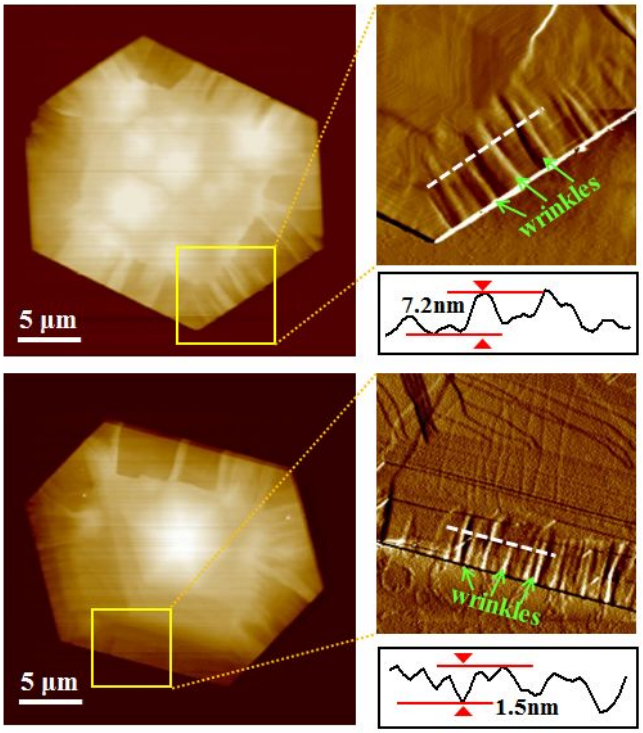

Figure S12. AFM images of SnS/SnS_2 core-shell heterostructures. Laterally epitaxial SnS_2 shows obvious wrinkles in the heterostructures induced by the interfacial stress from the lattice mismatch between SnS and SnS_2. The oscillated height profiles suggest the formation of wrinkles.